Dual role of ALCAM in neuroinflammation and blood–brain barrier homeostasis

Marc-André Lécuyer[a], Olivia Saint-Laurent[a], Lyne Bourbonnière[a], Sandra Larouche[a], Catherine Larochelle[a], Laure Michel[a], Marc Charabati[a], Michael Abadier[b], Stephanie Zandee[a], Neda Haghayegh Jahromi[b], Elizabeth Gowing[a], Camille Pittet[a], Ruth Lyck[b], Britta Engelhardt[b], and Alexandre Prat[a,c,1]

[a]Neuroimmunology Research Laboratory, Centre de Recherche du Centre Hospitalier de l'Université de Montréal (CRCHUM), Montreal, QC, Canada H2X 0A9; [b]Theodor Kocher Institute, University of Bern, 3012 Bern, Switzerland; and [c]Department of Neurosciences, Faculty of Medicine, Université de Montréal, Montreal, QC, Canada H3T 1J4

Edited by Lawrence Steinman, Stanford University School of Medicine, Stanford, CA, and approved December 9, 2016 (received for review August 29, 2016)

Activated leukocyte cell adhesion molecule (ALCAM) is a cell adhesion molecule found on blood–brain barrier endothelial cells (BBB-ECs) that was previously shown to be involved in leukocyte transmigration across the endothelium. In the present study, we found that ALCAM knockout (KO) mice developed a more severe myelin oligodendrocyte glycoprotein $(MOG)_{35–55}$–induced experimental autoimmune encephalomyelitis (EAE). The exacerbated disease was associated with a significant increase in the number of CNS-infiltrating proinflammatory leukocytes compared with WT controls. Passive EAE transfer experiments suggested that the pathophysiology observed in active EAE was linked to the absence of ALCAM on BBB-ECs. In addition, phenotypic characterization of unimmunized ALCAM KO mice revealed a reduced expression of BBB junctional proteins. Further in vivo, in vitro, and molecular analysis confirmed that ALCAM is associated with tight junction molecule assembly at the BBB, explaining the increased permeability of CNS blood vessels in ALCAM KO animals. Collectively, our data point to a biologically important function of ALCAM in maintaining BBB integrity.

multiple sclerosis | ALCAM | blood–brain barrier | EAE | tight junctions

The loss of blood–brain barrier (BBB) integrity is a hallmark of multiple sclerosis (MS). It is associated with the disorganization of junctional molecules that normally form complex apico-lateral molecular aggregates located in cholesterol-rich cell membrane regions called lipid rafts (1, 2). These molecules are highly regulated and are integral to the maintenance of the barrier. They can be divided into two major categories, the tight junction molecules (TJs) and the adherens junction molecules (AJs). The junctional adhesion molecules (JAMs), occludin, and the claudins are well-characterized transcellular TJs molecules, whereas Zonula occludens 1 and 2 (ZO-1 and -2) and cingulin are adaptor molecules located intracellularly that anchor the TJs to the actin filaments and regulate them spatiotemporally (3, 4). On the other hand, AJs are composed of cadherin molecules, such as vascular–endothelial (VE)-cadherin, and are linked to the cytoskeleton via proteins of the catenin family (α-, β-, p120) (5). Together, all these junctional proteins highly restrict leukocyte transmigration under homeostatic conditions.

Upon inflammation, cell adhesion molecules (CAMs), such as intercellular adhesion molecule 1 (ICAM-1) and vascular cell adhesion molecule 1 (VCAM-1), which are two of the most studied molecules involved in immune cell transmigration and recruitment to the brain and spinal cord, are up-regulated (6). A proof of concept that targeting CAMs for the treatment of autoimmune neuroinflammatory diseases (e.g., MS) was provided by the clinical success of Natalizumab, which targets the α4 integrin subunit of very late antigen-4 (VLA-4; binding partner to VCAM-1). However, the use of Natalizumab in clinical practice is limited due to the emergence of progressive multifocal leukoencephalopathy and rebound MS activity following withdrawal (7). Identifying novel key players involved during leukocyte diapedesis is thus crucial for the development of novel therapies that aim at decreasing leukocyte trafficking into the central nervous system (CNS) during neuroinflammation.

Although the roles of ICAM-1 and VCAM-1 during leukocyte transmigration in most vascular beds have been extensively studied (8–10), additional adhesion molecules have also been shown to partake in the transmigration process of encephalitogenic immune cells, including activated leukocyte cell adhesion molecule (ALCAM/CD166) (11, 12), melanoma cell adhesion molecule (MCAM) (13–15), mucosal vascular addressin cell adhesion molecule 1 (MAdCAM-1) (16, 17), vascular adhesion protein (VAP-1) (18, 19), Ninjurin-1 (20), and JAM-L (21). We have previously demonstrated that ALCAM is part of a group of adhesion molecules, found on BBB endothelial cells (BBB-ECs), that are involved in immune cell diapedesis (11, 12). ALCAM was initially discovered as a ligand for CD6, a costimulatory molecule involved in the formation of the immune synapse between lymphocytes and antigen-presenting cells (22–24). ALCAM can also bind to itself (homotypic ALCAM–ALCAM), although ALCAM–CD6 binding was later found to be the stronger of two possible interactions (25–27). Recently, both ALCAM and CD6 alleles were associated with an increased risk of developing MS (28–31).

In the current study, we found that ALCAM knockout (KO) mice develop a more severe active experimental autoimmune encephalomyelitis (EAE) due to an increased permeability of the BBB. We also present data indicating that ALCAM indirectly links junctional molecules to the cytoskeleton, suggesting that in addition to its role in transmigration, ALCAM regulates and maintains TJ stability by acting as an adaptor molecule.

Significance

Multiple sclerosis (MS) is an inflammatory disorder characterized by multifocal lesions in the central nervous system. These lesions are caused by infiltrating leukocytes that take advantage and/or actively participate in the disruption of the blood–brain barrier (BBB). In this study, the specific role of the adhesion molecule ALCAM (activated leukocyte cell adhesion molecule) present on BBB endothelial cells was assessed. We demonstrated that ALCAM knockout mice develop a more severe experimental autoimmune encephalomyelitis, the mouse model of MS, due to an increased permeability of the BBB. This phenotypic change is caused by a dysregulation of junctional molecules with which ALCAM indirectly binds, suggesting that in addition to its role in leukocyte transmigration, ALCAM regulates and maintains tight junction stability by acting as an adaptor molecule.

Author contributions: M.-A.L., R.L., B.E., and A.P. designed research; M.-A.L., O.S.-L., L.B., S.L., C.L., L.M., M.C., M.A., S.Z., N.H.J., E.G., C.P., and R.L. performed research; B.E. and A.P. contributed new reagents/analytic tools; M.-A.L. and R.L. analyzed data; and M.-A.L., R.L., B.E., and A.P. wrote the paper.

The authors declare no conflict of interest.

This article is a PNAS Direct Submission.

[1]To whom correspondence should be addressed. Email: a.prat@umontreal.ca.

This article contains supporting information online at www.pnas.org/lookup/suppl/doi:10.1073/pnas.1614336114/-/DCSupplemental.

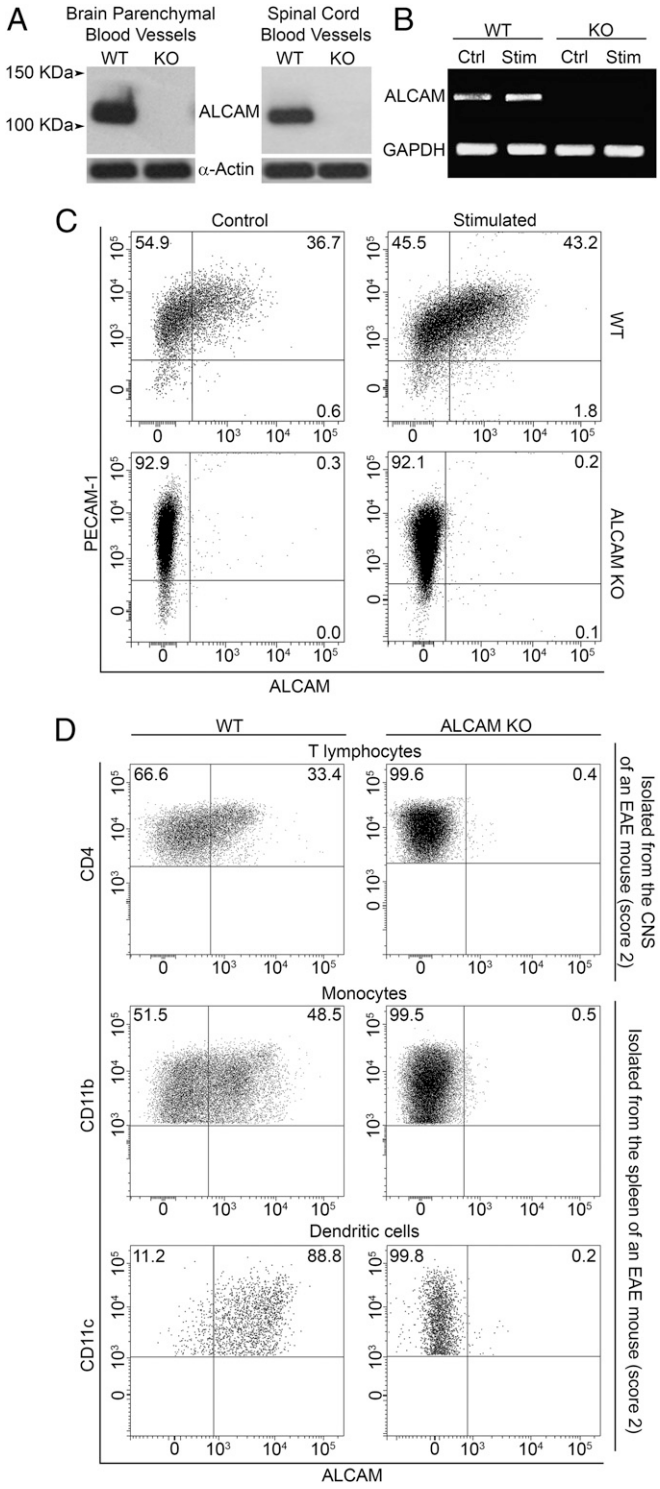

Fig. 1. Expression of ALCAM at the BBB and on immune cells. (*A*) Expression of ALCAM in freshly isolated blood vessels from the brain and spinal cord of WT and ALCAM KO mice, by Western blot (actin, control protein). Data are representative of $n = 5$ independent experiments. (*B*) RT-PCR analysis of *ALCAM* mRNA obtained from primary culture of mouse BBB-ECs (MBECs) from WT and ALCAM KO mice either resting (Ctrl) or treated with TNF and IFNγ (Stim, Stimulated). Data are representative of $n = 2$ independent experiments. (*C*) Expression of ALCAM and PECAM-1 on primary cultures of MBECs obtained from WT and ALCAM KO mice as assessed by flow cytometry. Data are representative of $n = 5$ independent experiments. (*D*) Expression of ALCAM on ex vivo $CD4^+$ T lymphocytes isolated from the CNS as well as $CD11b^+$ monocytes/macrophages and $CD11b^+CD11c^+$ dendritic cells isolated from splenocytes of ALCAM KO mice or their WT littermates during the early symptomatic phase of active EAE. Data are representative of $n = 3$ independent experiments.

Results

ALCAM Is Absent from BBB-ECs and the Immune Compartment of ALCAM KO Mice. To test the hypothesis that ALCAM plays an important role during leukocyte transmigration across the BBB, we used an ALCAM KO mouse. We first evaluated whether ALCAM was indeed absent in the animal cells. Using Western blot, ALCAM was detected on both freshly isolated brain and spinal cord microvessels from wild-type (WT) but not from ALCAM KO animals (Fig. 1*A*). These results were corroborated by the analysis of primary cultures of WT and ALCAM KO BBB-EC mRNA via RT-PCR. Following activation with TNF and IFNγ, *ALCAM* mRNA expression was up-regulated in EC cultures derived from WT animals, whereas *ALCAM* mRNA could not be detected in ALCAM KO samples (Fig. 1*B*). Similar results were obtained by flow cytometry analysis of PECAM-1^+ BBB-EC primary cultures (Fig. 1*C*). This confirmed the absence of ALCAM on BBB-ECs and thus allowed us to use ALCAM KO CNS blood vessels to study the role of ALCAM in transmigration.

Next, we assessed by flow cytometry the expression of ALCAM on ex vivo $CD4^+$ T lymphocytes isolated from the CNS of early symptomatic active EAE animals as well as $CD11b^+$ monocytes/macrophages and $CD11b^+CD11c^+$ dendritic cells isolated from the spleen of the same animals. Whereas myeloid cells of WT animals express high levels of ALCAM even in resting state, T lymphocytes express low to intermediate levels of ALCAM only once highly activated (Fig. 1*D*). Resting or activated T lymphocytes do, however, constitutively express CD6, which is a costimulation marker and one of the ligands of ALCAM (Fig. S1 *A* and *B*). Naïve ALCAM KO animals had normal absolute numbers, proportion, and distribution of peripheral immune cells in the spleen, lymph nodes (LNs), and thymus, compared with their WT littermates (Fig. S1 *C–J* and Fig. 2 *B* and *C*). Nevertheless, to assess the effect of ALCAM deficiency on lymphocyte proliferation in more detail, we conducted in vitro proliferation assays using WT CD4 T lymphocytes in combination with WT or ALCAM-deficient antigen-presenting cells. Both mixed leukocyte reactions and control assays showed similar percentages of cellular proliferation (50.9 ± 3.2% and 51.6 ± 2.4%, respectively). Likewise, no significant difference was observed in the production of IL-17 and IFNγ by CD4 T lymphocytes (IL-17: WT, 20.9 ± 5.9%, and KO, 23.4 ± 7.3%; IFNγ: WT, 26.1 ± 4.7%, and KO, 24.7 ± 3.2%). These data confirmed results obtained beforehand using anti-ALCAM blocking antibodies (11), demonstrating that the absence of ALCAM does not significantly influence the activation of lymphocytes and in vivo immune homeostasis.

ALCAM KO Mice Develop a More Severe Active EAE Associated with a Significant Increase in Proinflammatory Leukocyte Infiltrating the CNS. To assess the role of ALCAM during the pathogenesis of EAE, active EAE was induced in WT and ALCAM KO mice using myelin oligodendrocyte glycoprotein $(MOG)_{35–55}$ in complete Freund's adjuvant (CFA). As opposed to what we had expected based on previous publications (11, 24), ALCAM KO mice developed more severe clinical symptoms [area under the curve (AUC): WT, 86.48 ± 6.80; ALCAM KO, 117.6 ± 7.21], showing a diminished remission and often an earlier disease onset (1 d before their WT littermates) (Fig. 2*A*). Additional active EAE experiments induced with recombinant human MOG corroborated these results (Fig. S2*A*). Furthermore, these observations were made in two different animal facilities using independently bred ALCAM KO mice and their WT littermates, demonstrating the certainty of the outcome. Although the absolute number of immune cells found

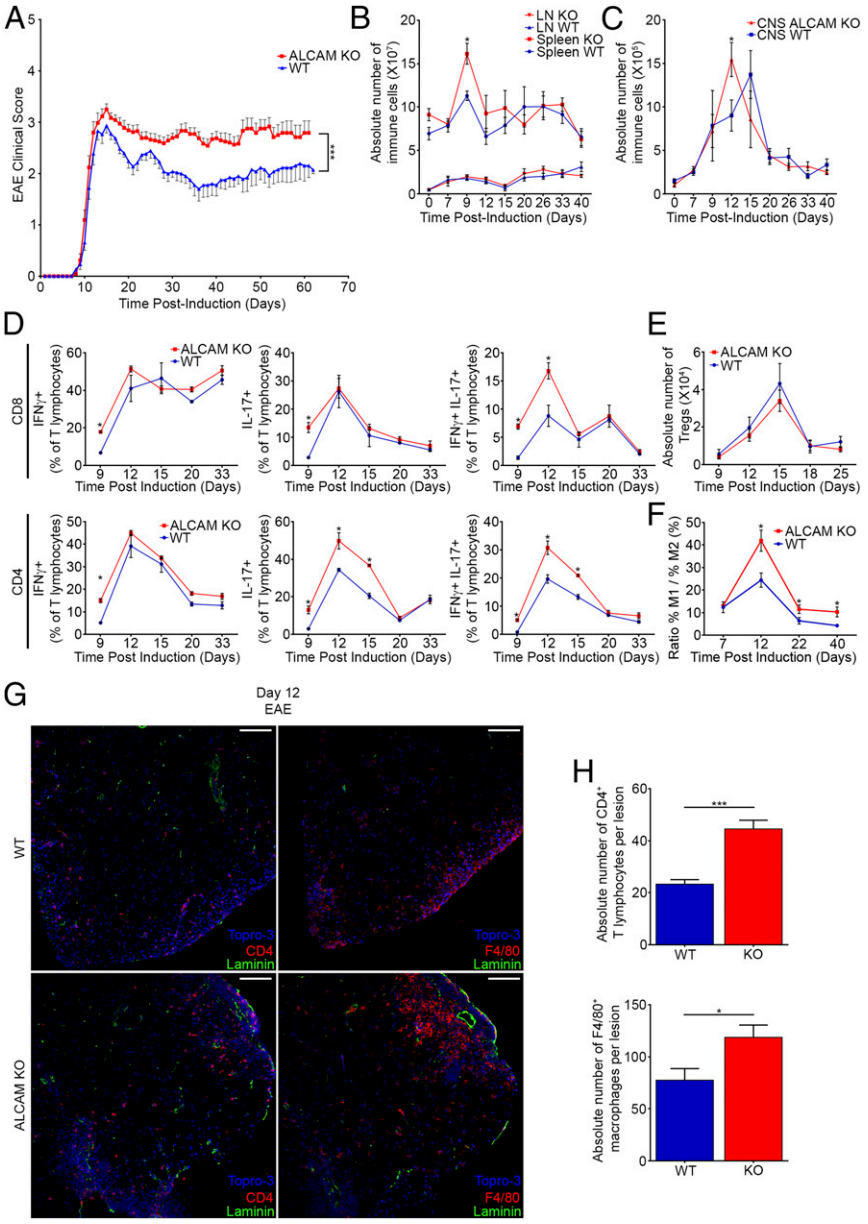

Fig. 2. ALCAM KO mice develop a more severe active EAE. (*A*) Mean cumulative clinical EAE score from $MOG_{35–55}$–immunized C57BL/6 WT and ALCAM KO mice. Data shown are the mean ± SEM of 40 mice per group and representative of $n = 12$ independent experiments. Absolute numbers of immune cells isolated from the spleens and LNs (*B*) or from the CNS (*C*) of WT and ALCAM KO mice at different dpi of EAE. Data shown are the mean ± SEM of 3–12 animals per time point and representative of $n = 8$ independent experiments. (*D*) Percentage of IFNγ-, IL-17–, or IFNγ and IL-17–expressing $CD4^+$ and $CD8^+$ T lymphocytes isolated from the CNS of WT and ALCAM KO mice at different dpi of EAE, as assessed by flow cytometry. Data shown are the mean ± SEM of 3–5 animals per time point and representative of $n = 5$ independent experiments. (*E*) Absolute numbers of $CD4^+CD25^+FOXP3^+$ regulatory T lymphocytes infiltrating the CNS of ALCAM KO and WT mice at different dpi of EAE, as assessed by flow cytometry. Data shown are the mean ± SEM of 3–6 animals per time point and representative of $n = 3$ independent experiments. (*F*) Prevalence of M1 monocytes/macrophages relative to M2 subtype isolated from the CNS of WT and ALCAM KO mice at different dpi of EAE, as assessed by their expression of CD11b, CD43, CD206, Ly6C, IL-10, and IL-12 by flow cytometry. Data shown are the mean ± SEM of 4–10 animals per time point pooled from three independent experiments. (*G*) Immunofluorescent staining of laminin (green), TOPRO-3 (nuclei, blue), and CD4 or F4/80 (red) in spinal cord sections of ALCAM KO and WT mice at day 12 postinduction of EAE. (Scale bar, 100 μm.) Images shown are representative of nine sections per animal and representative of $n = 4$ animals per group. (*H*) Absolute numbers of $CD4^+$ T lymphocytes and $F4/80^+$ macrophages observed per lesion. $n = 10–15$ lesions assessed from three animals per group. $^*P \leq 0.05$, $^{***}P \leq 0.001$.

in the draining inguinal LNs of both groups were virtually identical throughout the disease course, the absolute number of splenocytes was significantly higher in ALCAM KO animals after 9 d post-induction (dpi) (Fig. 2*B*). On the other hand, the highest absolute number of immune cells infiltrating the CNS of ALCAM KO mice occurred at 12 dpi, 3 d earlier than in their WT littermates (Fig. 2*C*). Of those CNS-infiltrating immune cells, $IFN\gamma^+$, $IL\text{-}17^+$, and $IFN\gamma^+/IL\text{-}17^+$ CD4 and CD8 T lymphocytes were found to enter the CNS of ALCAM KO animals earlier and in greater number than in WT animals, as assessed by flow cytometry (Fig. 2*D*). In addition, the number of $CD4^+CD25^+FOXP3^+$ regulatory T lymphocytes was found to be similar throughout the disease process in both ALCAM KO and WT CNS (Fig. 2*E*), which suggests that the increased disease severity observed in ALCAM KO mice was not due to a deficiency in the immune regulatory system. Finally, and importantly, we did not observe differences in cytokine production in the periphery (Fig. S2*B*), suggesting that enhanced and early recruitment of encephalitogenic lymphocytes in the CNS of ALCAM KO animals was not caused by an enhanced number of circulating activated peripheral immune cells.

Although EAE is mainly a CD4 T lymphocyte-driven disease, myeloid cells also play a crucial role both in the establishment of the disease and in the remission phase. Hence, we have assessed by flow cytometry the ratio of M1 (proinflammatory) versus M2 (anti-inflammatory/tissue repair) monocytes/macrophages present in the CNS. As expected from the ongoing increased clinical scores, ALCAM KO mice had a higher M1 over M2 ratio at the peak of disease (12 dpi) as well as in the chronic phase of the disease (Fig. 2*F*). Collectively, these results were corroborated by in situ immunofluorescence confocal microscopy of spinal cord material from ALCAM KO and WT animals harvested at 12 dpi (score 3.0 and 2.5, respectively). Immunostainings for CD4 and F4/80 in conjunction with panlaminin confirmed the significant increase in the number of helper T lymphocytes and macrophages in the CNS of ALCAM KO EAE mice compared with WT animals (Fig. 2 *G* and *H*).

The Absence of ALCAM on BBB-ECs Increases EAE Disease Severity. Different CAMs (i.e., ICAM-1 and VCAM-1) can compensate for the lack of specific CAMs in KO animals (32–34). Therefore, we have chosen to compare, by flow cytometry, the expression of other CAMs on primary cultures of WT and ALCAM KO mouse CNS ECs under resting or stimulated conditions (TNF and IFNγ). Although we confirmed that some CAMs are up-regulated upon inflammation, we could not demonstrate the presence of such a compensatory mechanism in ALCAM KO ECs (Fig. 3*A*). MCAM, Ninjurin-1, and CD62E, previously shown to be involved in the recruitment of specific immune cell types to the CNS (14, 15, 20, 35, 36), were also assessed and showed no significant differences between ALCAM KO and WT mouse BBB-ECs (MBECs) either in resting or stimulated conditions (Fig. S3).

We then performed passive (adoptive transfer) EAE by injecting WT MOG-reactivated splenocytes into both WT and ALCAM KO mice (Fig. 3*B*). ALCAM KO recipients demonstrated the first sign of symptoms 2 d earlier than their WT littermates and had higher clinical scores at peak of disease and subsequently during the remission phase (AUC: WT recipients, 21.43 ± 1.94, and ALCAM KO recipients, 38.06 ± 5.03). The disease incidence rate was also slightly more elevated in ALCAM KO recipients compared with WT with 100% and 95%, respectively. In addition, the absolute numbers of CNS-infiltrating immune cells were higher in ALCAM KO recipients after 12 d following cell transfer, corroborating the clinical scores (Fig. 3*C*). From these immune cells, the percentage of $CD4^+$ T lymphocytes was higher in ALCAM KO, whereas the percentage of $CD8^+$ T lymphocytes was higher in the WT recipients (Fig. 3*D*). As expected, the percentage of $ALCAM^+$ leukocytes was lower in ALCAM KO animals, as only the donor cells expressed that protein. However, it demonstrates that only roughly 20% of $CD4^+$ T lymphocytes and $CD11b^+$ monocytes present in the CNS of ALCAM KO originated from the donor cells (Fig. 3*D*). Although the percentages of CD4 and CD8 T lymphocytes were different in the two recipient groups, the percentages of those cells positive for IFNγ or IL-17 were similar, with the exception of

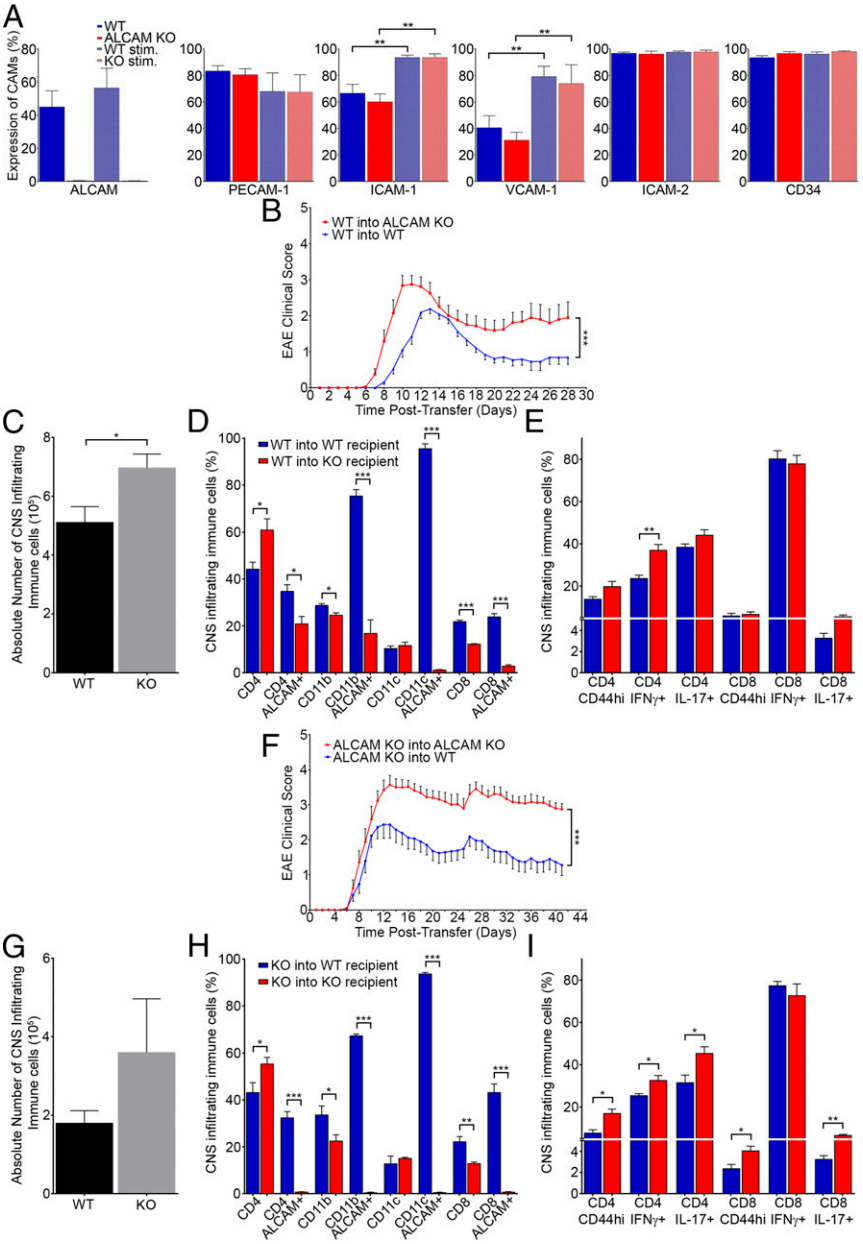

Fig. 3. The absence of ALCAM on BBB-ECs increases EAE disease severity. (*A*) Expression of CAMs (ALCAM, PECAM-1, ICAM-1, VCAM-1, ICAM-2, and CD34) on primary culture of MBECs under resting or stimulated (stim.; TNF and IFNγ) conditions, isolated from WT and ALCAM KO mice, as assessed by flow cytometry. $n = 4$ independent experiments using four primary cultures. (*B*) Mean cumulative EAE clinical score of WT and ALCAM KO mice adoptively transferred with $MOG_{35–55}$–reactivated WT splenocytes. Data shown are representative of $n = 3$ independent experiments, 20 animals per group. (*C–E*) Characterization of immune cells infiltrating the CNS of WT or ALCAM KO animals in the adoptive transfer EAE experiment, at 12 d posttransfer (shown in *B*). (*C*) Absolute numbers of immune cells isolated from the CNS of recipient mice. (*D* and *E*) Percentage of CNS-infiltrating immune cells expressing the surface markers CD4, CD11b, CD11c, and CD8 and percentage of $ALCAM^+$, CD44hi, $IFNγ^+$, and $IL\text{-}17^+$ cells gated on the previous surface markers. Data shown are the mean ± SEM of 3–4 animals per group and representative of three transfer experiments. (*F*) Mean cumulative EAE clinical score of WT and ALCAM KO mice adoptively transferred with $MOG_{35–55}$–reactivated ALCAM KO splenocytes. Data shown are representative of $n = 3$ independent experiments, with 26 WT and 20 ALCAM KO mice per group. (*G–I*) Characterization of immune cells infiltrating the CNS of WT or ALCAM KO animals in the adoptive transfer EAE experiment at 12 d post-transfer (shown in *F*). (*G*) Absolute numbers of immune cells isolated from the CNS of recipient mice. (*H* and *I*) Percentage of CNS-infiltrating immune cells expressing the surface markers CD4, CD11b, CD11c, and CD8 and percentage of $ALCAM^+$, CD44hi, $IFNγ^+$, and $IL\text{-}17^+$ cells gated on the previous surface markers. Data shown are the mean ± SEM of four animals per group and representative of three transfer experiments. $^*P \le 0.05$, $^{**}P \le 0.01$, $^{***}P \le 0.001$.

IFNγ$^+$CD4$^+$ T lymphocytes (Fig. 3*E*). Overall, this means that more proinflammatory cytokine-secreting CD44hiCD4$^+$ T lymphocytes were present in the CNS of ALCAM KO at day 12, whereas the reverse was true for CD8 T lymphocytes. Ultimately, this transfer experiment allowed us to hypothesize that the absence of ALCAM on BBB-ECs might destabilize the BBB and therefore explain the increased EAE severity observed in MOG-induced active EAE.

We then performed the reverse transfer experiment, in which ALCAM KO splenocytes were injected into either ALCAM KO naïve recipients or their WT littermates. The disease onset was slightly earlier in ALCAM KO recipients, and animals developed more severe EAE scores compared with WT recipients (AUC: ALCAM WT recipients, 60.85 ± 8.89, and ALCAM KO recipients, 90.67 ± 10.69) (Fig. 3*F*). The disease incidence was also higher in ALCAM KO mice with 83%, compared with 72% for the WT. Although the absolute number of CNS-infiltrating immune cells were not significantly higher in ALCAM KO recipients after 12 dpi, a noticeable trend can be observed, albeit with a large variability (Fig. 3*G*). Similar to the WT to KO/WT transfer experiment, a higher percentage of CD4$^+$ T lymphocytes could be observed by flow cytometry in the CNS of ALCAM KO recipients, whereas a smaller percentage of CD8$^+$ T lymphocytes was present (Fig. 3*H*). Because ALCAM$^+$ leukocytes present in the CNS can only originate from the recipient, virtually no ALCAM$^+$ signal was detected in ALCAM KO animals, as expected (Fig. 3*I*). Finally, the percentages of CD4 T lymphocytes positive for IFNγ or IL-17 or expressing high levels of CD44 were greater in ALCAM KO recipients (Fig. 3*J*). Similar results were obtained while gating on CD8$^+$ T lymphocytes, with the exception of IFNγ, which was expressed at equally high levels in both groups (Fig. 3*J*). Overall, this transfer experiment corroborated our hypothesis that ALCAM expression on the BBB helps in maintaining its integrity.

The BBB of ALCAM KO Animals Is More Permeable. We next tested the integrity of the ALCAM KO BBB in vitro and in vivo. Using a transendothelial electrical resistance (TEER) assay, we first demonstrated that confluent monolayers of primary mouse brain microvascular endothelial cells (pMBMECs) from ALCAM KO mice were significantly more permeable (i.e., less resistant) than their WT counterpart (Fig. 4*A*). Whereas TEER measurements can clearly assess the integrity of the endothelial barrier, we also decided to corroborate the result using BSA and 10-kDa dextran as permeability markers in a modified in vitro Boyden chamber assay in which confluent monolayers of MBECs were grown on the insert. This tracer diffusion assay demonstrated that ALCAM KO MBECs have a higher permeability coefficient compared with WT cells (Fig. 4*B*) when using either resting MBECs or MBECs stimulated with TNF and IFNγ. Next, we wanted to confirm these in vitro data with an in vivo approach. Using different sizes of fluorescent dextran markers injected intravenously, we measured the accumulation of these tracers in the CNS (and indirectly the permeability of the BBB) in naïve animals as well as in EAE mice at 7 and 10 dpi. Although CNS vessels of naïve ALCAM KO animals were not more permeable than those from control WT littermates, CNS vessels from presymptomatic ALCAM KO EAE animals were significantly more permeable to the small 3-kDa dextran marker compared with vessels from WT littermates (Fig. 4*C*); the differences in vascular permeability for larger molecular weight dextran markers became apparent at 10 dpi, corresponding to the time of disease onset (Fig. 4*C*). Furthermore, immunofluorescent staining performed on tissue of 1-y-old animals showed higher levels of IgG and fibrinogen deposition in the CNS of ALCAM KO animals compared with WT controls (Fig. S4 *B* and *C*). In addition, extensive astroglial activation in these ALCAM KO animals was observed by an increased expression of GFAP (Fig. S4*A*), possibly a reflection of astrocyte activation by blood product percolating across the defective BBB, including fibrin. Together, these results provide the proof that ALCAM dysregulation leads to an increased permeability of the BBB.

Junctional Molecule Expression at the BBB Is Altered in ALCAM KO Animals. To explain the increased BBB permeability in ALCAM KO, we assessed the expression of junctional molecules. Using immunofluorescence confocal imaging, we evaluated the organization of TJ and AJ molecules as well as their expression levels based on the maximum fluorescence intensity. Analysis of spinal cord sections from naïve animals revealed that the expression of the TJ proteins occludin and ZO-1 as well as the AJ protein α-catenin was reduced in ALCAM KO mice (Fig. 4*D*). We further demonstrated that claudin-5, p120, and ZO-1 were also downregulated in situ, at the level of the BBB in spinal cord sections of ALCAM KO naïve animals, whereas the expression of PECAM-1 and β-catenin was similar (Fig. 4*E*). Similarly, we compared the expression of junctional molecules in MBEC cultures. Using the same method, α-/β-catenin, claudin-5, ZO-1, and VE-cadherin expression were shown to be reduced in vitro, whereas the expression of PECAM-1 and ICAM-1 were comparable (Fig. 4*F*). Although we also analyzed the spinal cord of EAE animals, the results were much more variable depending on the clinical scores. Furthermore, the presence of massive perivascular infiltrates, the disorganization of junction molecules by the immune cells, and the presence of debris in demyelinating lesions made it more challenging to analyze.

ALCAM Is Linked to Junctional Molecules. Having established that the integrity of ALCAM KO BBB is defective due to the disorganization and reduced expression of junctional molecules, we next elected to confirm a possible molecular interaction between ALCAM and junctional proteins. To do so, we performed an immunoprecipitation of ALCAM on MBEC protein lysates (Fig. 5*A*). A proteomic analysis was performed by liquid chromatography–tandem mass spectrometry on the proteins pulled down with ALCAM. A list of the most abundant proteins was made, and from that list, probable ALCAM binding partners were identified. Eight of those were subsequently verified by Western blot. We demonstrated that an isoform of ZO-2, cingulin, TRIO and F-actin binding protein (TRIOBP, TARA), coronin 1C, β-actin, and pan-tropomyosin (TPM) were all linked directly or indirectly to ALCAM (Fig. 5*B*). Although present on the list, both ZO-1 and occludin were not detected by Western blot in the proteins pulled down with ALCAM (Fig. 5*B*). Similarly, ezrin and syntenin-1, which have been recently identified as intracellular ALCAM binding partners in dendritic cells, were not detected in the pulled-down protein lysate (Fig. 5*B*) (37). These results suggest that ALCAM is present in the intercellular junctions and stabilizes the junctional molecular complexes by binding to cellular structural fibers such as actin and myosin.

Discussion

In previous studies, ALCAM has been shown to be expressed on BBB-ECs and its ligands, CD6 and ALCAM, on activated and resting leukocytes (11, 12, 38). Furthermore, we have previously demonstrated that physical hindrance of ALCAM during active EAE, using anti-ALCAM blocking antibodies, delays the progression and reduces the severity of the disease, while also partially preventing the infiltration of leukocytes in the CNS (11). In addition, several groups have demonstrated the involvement of ALCAM in leukocyte transmigration across human BBB-ECs or MBECs (11, 12, 38–41).

Using a constitutive ALCAM KO animal, we now provide evidence that following the induction of active EAE, ALCAM-deficient mice progress to a higher clinical score, with a significantly more severe ascending paralysis than their WT littermates. Interestingly, an increase in the absolute number of splenocytes can be observed in ALCAM KO animals at 9 dpi, compared with WT

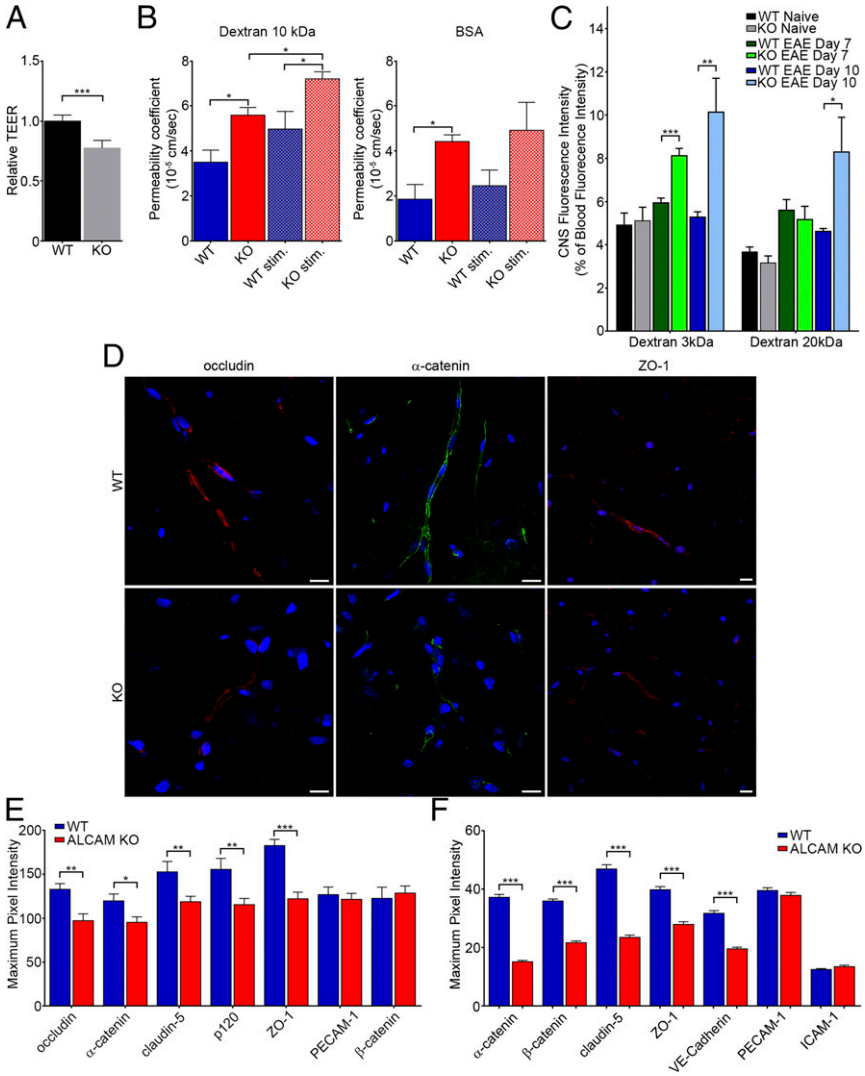

Fig. 4. ALCAM KO mice exhibit disorganized TJ molecules, which translates into an increase in transendothelial cell permeability. (*A*) TEER values of confluent monolayers of pMBMECs isolated from WT or ALCAM KO mice, expressed relative to WT values (1.0). Data shown are the mean ± SEM of seven independent experiments performed in triplicates. (*B*) Permeability coefficient of 10-kDa dextran and BSA across monolayers of MBECs, in vitro, from WT or ALCAM KO mice, either untreated or treated with TNF and IFNγ (stim.). Data shown are the mean ± SEM of 3–4 replicates per conditions and representative of $n = 3$ independent experiments. (*C*) In vivo BBB permeability using i.v. injected fluorescently labeled dextran (3 and 20 kDa) at different time points during EAE in WT and ALCAM KO mice. Data are expressed as a percentage of blood fluorescence intensity and measured by spectrofluorometer. Data shown are the mean ± SEM of 5–15 replicates per conditions pooled from $n = 3$ independent experiments. (*D*) Immunofluorescent staining of occludin (red; *Left*), α-catenin (green; *Center*), and ZO-1 (red; *Right*) in spinal cord sections of naïve ALCAM KO and WT mice. Nuclei, blue. (Scale bar, 20 μm.) Data are representative of five sections per animal and $n = 4$ animals per group. (*E*) Maximum pixel intensity analysis of junctional molecules in naïve ALCAM KO and WT spinal cord sections, as assessed by confocal microscopy. $n = 25$–65 blood vessels per group. (*F*) Maximum pixel intensity analysis of junctional molecules in primary culture of MBECs. $n = 160$–260 cell junctions per group. $^{*}P \leq 0.05$, $^{**}P \leq 0.01$, $^{***}P \leq 0.001$.

littermates. As we have shown that the absence of ALCAM does not significantly impact lymphocyte activation, this observation could potentially be explained by the presence of CNS antigens filtering out of the CNS and reaching the peripheral secondary lymphoid organs at an earlier time point in ALCAM KO animals, following CNS injury. Inflammatory factors could similarly permeate outside the CNS due to the weaker BBB in ALCAM KO animals. These factors and neoantigens could lead to an exaggerated activation of the peripheral immune system and thus subsequently strengthen the inflammatory reaction. Irrespective of the reasons behind the increased absolute number of splenocytes at 9 dpi in ALCAM KO mice, a significantly higher number of proinflammatory immune cells are found in the CNS of these animals at the peak of disease, presumably also due to a weaker BBB. From this population of CNS-infiltrating immune cells, a higher percentage of T lymphocytes are secreting the proinflammatory cytokines IFNγ and IL-17 compared with those found in WT mice. Similarly, "M1" macrophages (proinflammatory) are found in higher number in the CNS of ALCAM-deficient animals. However, regulatory T lymphocytes are found in similar numbers in the CNS of ALCAM KO and WT animals despite the fact that a previous study demonstrated the involvement of ALCAM during the recruitment of Tregs into tumor tissues (42). Although these EAE results were unexpected, we also found enriched populations of $ALCAM^{+}$ leukocytes infiltrating the CNS of WT EAE mice, compared with peripheral immune compartments, suggesting that ALCAM expression on encephalitogenic immune cells is important during the transmigration process, which is in line with previous literature.

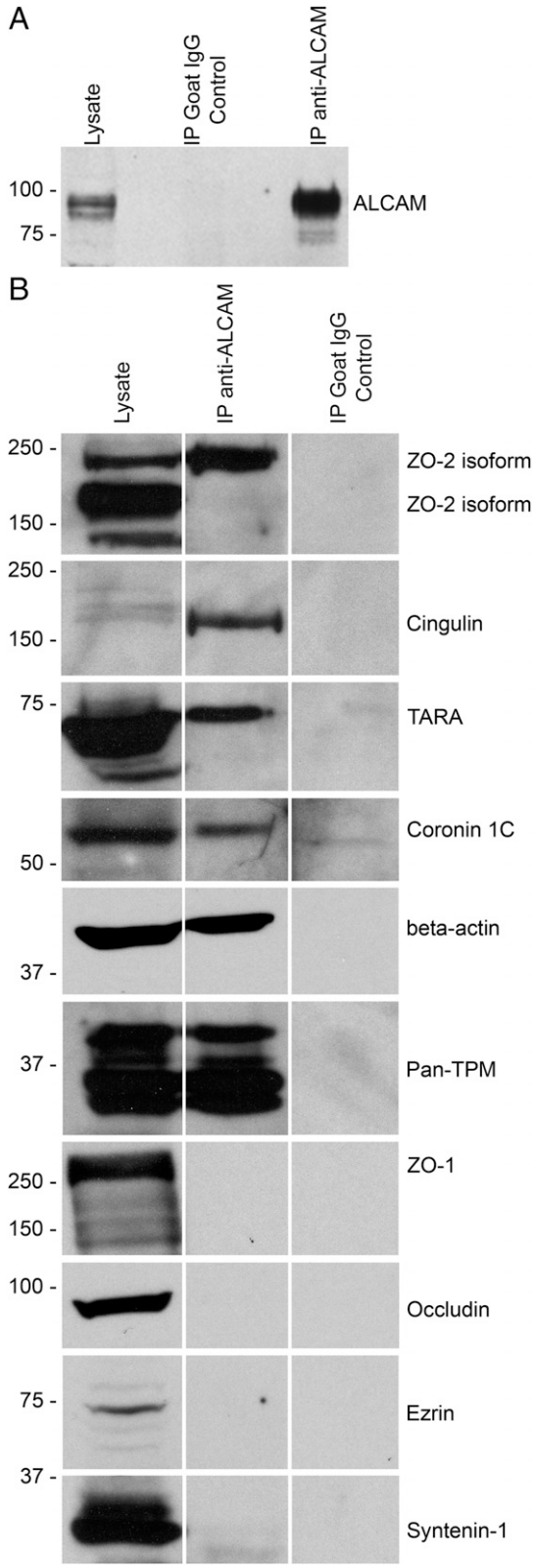

Fig. 5. ALCAM binds directly and indirectly to TJs. (*A*) Expression of ALCAM protein in whole-cell lysate from MBECs, in the control immunoprecipitation using nonspecific goat IgGs and in the ALCAM immunoprecipitation (IP) sample, by Western blot. (*B*) Immunoblot for ZO-2 (isoforms ± 160 kDa), cingulin (160 kDa), TARA (68 kDa), coronin 1C (57 kDa), β-actin (42 kDa), pan-TPM (isoforms ± 33 kDa), ZO-1 (240–260 kDa), occludin (65–80 kDa), ezrin (69 kDa), and syntenin-1 (33 kDa) on the ALCAM pull-down lysate (*Center*), the corresponding MBEC total cell lysate (*Left*), and the control IP (*Right*).

Although some groups have shown a role for the heterotypic interaction ALCAM–CD6 in the proliferation of CD4 T lymphocytes (24, 29), we have previously established that ALCAM blockade does not influence in vitro proliferation and activation of human CD4 T lymphocytes (11). In the current study, we now provide in vivo evidence that genetic neutralization of ALCAM does not affect the peripheral immune system homeostasis nor T-cell proliferation in mouse. Therefore, it is unlikely that the impeded CD6 signaling pathways on T lymphocytes or a compensatory mechanism are responsible for the increased clinical score of ALCAM KO mice during active EAE.

Using transfer EAE experiments, where MOG-reactive WT splenocytes are transferred into ALCAM KO animals, we confirmed that ALCAM genetic neutralization in the recipient mice leads to a more severe disease and to an increased number of encephalitogenic leukocytes infiltrating their CNS compared with WT littermates. To rule out the possibility that increased immune cell infiltration could be mediated by the up-regulation of additional CAMs (ALCAM-independent pathways) in ALCAM KO animals, we assessed the expression of other CAMs on BBB-ECs and found no evidence of compensatory mechanisms. However, we could demonstrate a significant reduction of BBB integrity in ALCAM-deficient animals, as supported by a reduced TEER and an increased extravasation of fluorescent molecules, both in vitro and in vivo. This altered BBB integrity was associated with a dysregulation of TJ and AJ molecules in the CNS of ALCAM KO animals, including occludin, α-catenin, β-catenin, claudin-5, ZO-1, p120, and VE-cadherin. Differences found between in vitro and in vivo experiments might be the result of complex intrinsic glial cells' contribution to the development of a tightly controlled BBB (6), which concurrently helps delineate the inherent limits of in vitro assays. Collectively, these experiments thus demonstrate that ALCAM-deficient animals have a dysregulated BBB.

Based on previous studies demonstrating the presence of ALCAM in lipid rafts of both human BBB-ECs and MBECs (11, 38) and the localization of human ALCAM immunostaining with BBB-EC lateral junctions (12), we hypothesized that, in homeostatic conditions, ALCAM is located within intercellular structures and might therefore directly or indirectly bind to junctional molecules. As such, ALCAM would be similar to PECAM-1, CD99, JAMs, and MCAM, which are present within BBB-EC junctions but also mediate immune cell transmigration (15, 43–46). Although Masedunskas et al. (40) have previously reported the presence of ALCAM in EC junctions using pulmonary microvascular ECs transfected with rat ALCAM-GFP, the localization of endogenous ALCAM in BBB-EC junctions had still not been established. The findings presented herein, using primary cultures of MBECs, demonstrate that ALCAM is localized with intercellular junctional proteins and also bind to the TJ adaptor molecules ZO-2 and cingulin, confirming a direct link between ALCAM and intracellular TJ adaptor molecules. In contrast, transmembrane TJ molecules (occludin, the JAMs, and the claudins) were not pulled down with ALCAM, which suggests that ALCAM binds or recruits cytoplasmic adaptor molecules to junctional complexes but does not directly interact with transmembrane TJ proteins. Using the pulled-down protein lysate, we also identified actin-binding proteins TARA and coronin 1C, which, along with the presence of β-actin and TPM proteins, confirm previous studies and provide further evidence demonstrating that ALCAM is directly linked to the actin cytoskeleton (37, 47, 48). The study by Nelissen et al. (47), in particular, demonstrated that clustering of ALCAM is essential for cell adhesion and that it is mediated partly by actin polymerization. Their study also suggested a strengthening of the cytoskeleton linkage following ALCAM ligand binding. As such, ALCAM might participate in cytoskeletal rearrangements at the level of the TJs. In addition, a study by Zimmerman et al. (49) suggested that PKCα plays a dominant role in modulating the cytoskeleton-dependent avidity of ALCAM by controlling directly cytoskeleton reorganization.

Thus, the interactions between ALCAM and the cytoskeleton are possibly intricately controlled by one another, favoring the stabilization of intercellular junctions in the presence of ALCAM. Collectively, the localization of the above mentioned pulled-down proteins, along with ALCAM, to lipid rafts is also consistent with the current literature, which associates these cell membrane microdomains with the formation of complex macromolecular structures involved in immune cell transmigration (selectins, ICAM-1, VCAM-1, etc.), intercellular junction formation, cytoskeleton anchoring, and intracellular signaling pathways (50–52).

Although no proteins of the catenin or cadherin families were identified in the proteomic list, an indirect link with ALCAM via ZO-2 could still be possible in homeostatic condition. Additional proteins previously shown, by Tudor et al. (37), to bind ALCAM intracellularly, such as ezrin and syntenin-1, were not pulled down during our experiments. The discrepancy between their findings and the data presented herein could be explained by their use of the K562 cell line combined with the transfection of modified ALCAM proteins, as opposed to endogenous ALCAM obtained from primary MBECs. Interestingly, although the cytoplasmic tail of ALCAM contains clusters of positively charged amino acid residues that typically interact with members of the ezrin/radixin/moesin (ERM) family, a study performed with pulmonary microvascular ECs found no association between ALCAM and ERM protein family members, corroborating our results (53). Furthermore, Gilsanz et al. (54) have recently reported that ALCAM forms a complex with the tetraspanin molecule CD9 and the "sheddase" ADAM17, which together regulate ALCAM expression and activity (55). Although CD9 is highly expressed on ECs (56), we were unable to confirm the link between ALCAM and CD9. However, the existence of such a bond in BBB-ECs is still a possibility, as a different cell activation state might be necessary to observe the link. Technical differences in the protocols used could also explain the discrepancy.

Collectively, our data demonstrate that ALCAM KO mice develop a more severe active EAE, which can be explained by an increased permeability of their BBB. This loss in BBB integrity is due to a dysregulation of junctional molecules caused by the lack of ALCAM at the level of the TJ molecules. Our results also show that ALCAM indirectly and directly links junctional molecules to the actin cytoskeleton, suggesting that, in addition to its role during leukocyte extravasation, ALCAM regulates and maintains TJ stability by acting as an adaptor molecule. Most importantly, mouse and human ALCAM molecules are 93% homolog, and the binding regions, the transmembrane region, and the intracytoplasmic tail are all highly conserved between most vertebrates, suggesting that the results reported herein may also be applicable to human.

Methods

ALCAM KO Mice. The ALCAM KO C57BL/6 mice (Alcamtm1Jawe) were generously provided by Joshua A. Weiner, Departments of Biology and Psychiatry, The University of Iowa, Iowa City, IA (57). The founding animals were further backcrossed in our animal facility for seven generations. The weight of the animals matched those of aged-matched WT C57BL/6, and no gross abnormalities or phenotypes were apparent from the embryonic stage to adulthood, confirming the observation made by the group of J. A. Weiner (57). Animals were kept for a maximum of 1 y with no health issues, which suggests a normal life expectancy. All animal procedures were approved by the Centre de Recherche du Centre Hospitalier de l'Université de Montréal Animal Care Committee (N11023APs) and followed guidelines of the Canadian Council on Animal Care. All animal procedures executed in the B.E. laboratory were approved by the committee of animal experimentation of the Veterinary Department of the Kanton Bern (permit no. BE42/14) and are in keeping with institutional and standard protocols for the care and use of laboratory animals in Switzerland.

Active EAE Disease Induction and Scoring. EAE was induced in 6–9-wk-old female C57BL/6 mice, as previously published (14, 15). In brief, animals were immunized with 200 μg s.c. of $MOG_{35–55}$ (MEVGWYRSPFSRVVHLYRNGK; Alpha Diagnostic International) or recombinant human MOG in a 100-μL emulsion of CFA (4 mg/mL *Mycobacterium tuberculosis*; Fisher Scientific). On day 0 and day 2, Pertussis toxin (500 ng PTX, Sigma-Aldrich) was injected intraperitoneally (i.p.). The scoring system used was as follows: 0, normal; 1, limp tail; 2, slow righting-reflex; 2.5, difficulty walking/ataxia; 3, paralysis of one hindlimb (monoparalysis); 3.5, hindlimb monoparalysis and severe weakness in the other hindlimb; 4, paralysis of both hindlimbs (paraparalysis); 4.5, hindlimb paraparalysis and forelimb weakness; 5, moribund (requires sacrifice). Mice were scored by an investigator blinded to the transgenic group.

Active EAE in the B.E. laboratory was induced in 8-wk-old female mice with 200 μg of $MOG_{35–55}$ in IFAs (LabForce; Santa Cruz Biotechnology) supplemented with 4 mg/mL desiccated *M. tuberculosis* (H37RA; Difco/BD Biosciences/BD Clontech). A total of 300 ng of PTX (List; LuBioScience) per mouse was administered i.p. at days 1 and 3 postimmunization. Weights and clinical severity were assessed twice daily and scored as follows: 0, healthy; 0.5, limb tail; 1, hind leg weakness; 2, hind leg paraplegia; 3, hind leg paraplegia and incontinence.

Transfer EAE. Transfer EAE was performed as previously described (14). Briefly, active EAE was induced as described above except that PTX (500 ng) was only injected on day 0. On day 7, mice were killed and leukocytes were recovered from LNs and spleens as previously published (58). Cells isolated were cultured for 90 h in RPMI supplemented with 10% (vol/vol) FBS, glutamine, nonessential amino acids, Hepes, sodium–pyruvate, and β-mercaptoethanol. Reactivation of cells was performed in the presence of $MOG_{35–55}$, rhTGF-β, rmIL-6, rmIL-23, and rmIL-12 (R&D Systems). Fresh complete medium (20% of initial volume) with rmIL-23 (500% of initial concentration) was added to all cultures on day 2. Cells were then harvested, washed in Hank's balanced salt solution (HBSS), and then processed for analysis by flow cytometry. We injected 25×10^6 total leukocytes i.p. to all of the recipient female C57BL/6 animals. Recipient mice received a single dose of PTX i.p. (200 ng) on day 2 following transfer. The scoring system used was the same as described above.

MBECs/pMBMECs. Primary cultures of mouse brain parenchymal capillary ECs (MBECs) were prepared from 10 to 15 WT or ALCAM KO 7–9-wk-old female C57BL/6 mice. The brains were isolated without perfusion, and meninges/choroid plexuses were removed. The parenchymal tissue was minced and homogenized at low speed in a mechanical Dounce homogenizer. The homogenate was then digested in DMEM containing 0.7 mg/mL collagenase type II (Worthington Biochemical Corp.) and 39 U/mL DNase I (Worthington Biochemical Corp.) for 75 min at 37 °C. Myelin was removed by centrifugation at $1,000 \times g$ for 20 min in 20% BSA–DMEM (Sigma-Aldrich). The remaining pellet was then shaken for 1 h at 37 °C with a mixture of 1 mg/mL collagenase-dispase (Roche) and 39 U/mL DNase I in DMEM. The microvessels were separated from remaining glial cells and red blood cells using a 33% continuous Percoll gradient centrifuged at $1,000 \times g$ for 10 min. Microvessels were plated on six-well culture dishes coated with 5 μg/mL collagen type IV (Sigma-Aldrich). MBECs were cultured in DMEM supplemented with 20% (vol/vol) FBS (Sigma-Aldrich), 1 ng/mL basic fibroblast growth factor (Roche), 100 μg/mL heparin (Sigma-Aldrich), 1.4 μM hydrocortisone (Sigma-Aldrich), and 1 × antibiotic–antimycotic solution (Invitrogen). The media was replaced every 24 h during the first 3 d. Puromycin (10 μg/mL) (Sigma-Aldrich) was added to the media for the first 48 h of culture. After 72 h, 4 μg/mL puromycin was maintained in the culture media. A confluent monolayer was formed following 4–6 d in culture. MBEC culture expressed vascular endothelial–cadherin protein. No immune reactivity for α-smooth muscle actin, glial fibrillary acidic protein, or neuronal nuclei protein could be detected, confirming the absence of contaminating smooth muscle cells, astrocytes, and neurons, respectively. To stimulate ECs, mouse recombinant TNF (3 ng/mL) and IFNγ (60 ng/mL) (R&D Systems) were added to the culture media 24 h before the experimental procedure.

The isolation and culture of pMBMECs in the B.E. laboratory was performed as described before (9, 59).

Flow Cytometry Analysis. Extracellular and intracellular stainings were performed as previously described (14). Briefly, before intracellular cytokine staining (ICS), cells were activated for 5 h with 1 μg/mL ionomycin and 20 ng/mL phorbol 12-myristate 13-acetate (PMA) in the presence of 2 μg/mL brefeldin A (all from Sigma-Aldrich). After staining for surface antigens, cells were then fixed and permeabilized in 4% (wt/vol) paraformaldehyde with 0.1% (wt/vol) saponin in HBSS for 10 min at room temperature before proceeding to intracellular staining. Mouse immune cells isolated from LNs, spleen, and CNS were labeled with the following antibodies against surface markers: CD3, CD4, CD8, CD11b, CD11c, CD25, CD45, CD54/ICAM-1, and CD62E (from BD Biosciences); CD6 and CD44 (from eBioscience); CD31/PECAM-1, CD34, CD102/ICAM-2, CD106/VCAM-1, and CD146 (from Biolegend); CD166/ALCAM (FAB1172P from R&D); and Ninjurin-1 (custom made from BD Biosciences). For intracellular staining of mouse cytokines, the following antibodies specific for mouse were used: IL-17, GM-CSF, TNF, and IFN-γ (from BD Biosciences) and GzB and perforin (from eBioscience). Intranuclear stainings were performed using eBioscience fixation/permeabilization kit in combination with

anti-FOXP3 antibodies (eBioscience and BD Biosciences). Nonspecific background staining was assessed using appropriate fluorochrome-matched isotype antibodies. Cells were processed on the same day for analysis on a BD LSR II and data analyzed using BD FACSDiva software (BD Bioscience).

Flow Cytometry Analysis Strategy for M1–M2 Monocytes/Macrophages. Cells positive for CD45, CD11b, Ly6C^{hi}, and IL-12 (all from BD Biosciences) and negative for CD11c and CD43 (BD Biosciences), NK1.1 and IL-10 (BD Biosciences and Biolegend), and CD206 (Biolegend) were considered as M1 monocytes/macrophages or "classically activated" proinflammatory cells. Cells positive for CD45, CD11b, CD43, CD206, and IL-10 and negative for CD11c, NK1.1, Ly6C^{hi}, and IL-12 were considered as M2 monocytes/macrophages or "alternatively activated" anti-inflammatory cells.

In Vitro T Lymphocyte Proliferation Assay. Using Miltenyi Biotec magnetic beads and columns, CD4$^+$ T lymphocytes were isolated (negative selection) from the draining LNs of WT presymptomatic active EAE animals, and CD11b$^+$ monocytes were isolated (positive selection) from the spleen of both WT and ALCAM KO mice. T lymphocytes were labeled using the vital dye 5,6-carboxyfluorescein diacetate succinimidyl ester (CFSE) and were cultured in the presence of either WT or ALCAM KO monocytes for 4 d. The cytokine mixture and media used during in vitro reactivation of immune cells to induce passive EAE were used. T lymphocyte proliferation and cytokine production were assessed by flow cytometry.

Immunostaining of CNS Material and Cell Culture. Frozen sections of CNS specimens (brain and spinal cord) obtained from mice following rapid intracardiac perfusion were studied as previously described (60–62). First, EAE lesions, defined as areas of demyelination associated with intense perivascular immune cell infiltration, were identified by Luxol Fast Blue (LFB) and hematoxilin and eosin (H&E) staining. Sections adjacent to active lesions were selected for immunohistofluorescence. Following fixation in acetone for 10 min, sections were transferred to ethanol for 5 min, hydrated in PBS, and blocked with 10% species-specific serum of the secondary antibody hosts. Primary antibodies diluted in 3% serum were incubated for 1 h at room temperature or overnight at 4 °C. Following washes with PBS Tween 20 (0.05%), secondary antibodies were incubated 45 min at room temperature. Sections were then mounted using Mowiol reagent containing Topro-3 (Invitrogen, 1:400) when indicated. Each experiment included negative controls (incubation with secondary antibodies alone). For immunocytofluorescence, MBECs were trypsinized and transferred to Ibidi μ-slides VI 0.1 coated with collagen IV. Once the cells reached confluence, they were fixed with 70% ethanol for 5 min and then permeabilized with PBS Tween 20 (0.05%) for 5 min. The subsequent staining procedures were the same as above. The following primary antibodies were used: rabbit anti-laminin (1:2,000, Dako), rat anti-CD4 (1:70, BD Bioscience), rat anti-F4/80 (1:80, Biolegend), rabbit anti-occludin (1:50, Invitrogen), rabbit anti–α-catenin (1:40, Invitrogen), rabbit anti–claudin-5 (1:100, Invitrogen), goat anti-p120 (1:30, Santa Cruz), rabbit anti–ZO-1 (1:70, Invitrogen), rabbit anti–β-catenin (1:150, Invitrogen), rat anti–VE-cadherin (1:10, BD Bioscience), rat anti–PECAM-1 (1:300, BD Bioscience), rat anti–ICAM-1 (1:100, eBioscience), and rabbit anti-fibrinogen (1:1,500, Innovative Research). Fluorescence acquisition was performed using a Leica Confocal Microscope SP5 platform (Leica Microsystems). Image processing and analysis were done using Leica LAS AF and ImageJ (NIH) software.

RT-PCR. RT-PCR was performed as previously published (11). Briefly, total RNA was extracted from the primary culture of WT and ALCAM KO MBECs using the RNeasy Mini Kit and transcribed into cDNA using QuantiTect Reverse Transcription kit (both from Qiagen) according to the manufacturer's instructions. ALCAM- and GAPDH-specific primers were used for the PCR.

Immunoprecipitation. MBEC homogenates were prepared from P0 monolayers in T75 flasks. The cells were washed three times with room temperature PBS and then scrapped and transferred to 15-mL tubes in PBS. The cells were precipitated by centrifugation at 400 × *g* for 10 min at room temperature. The supernatant was removed, and the cell pellets were homogenized with 200 μL of ice-cold RIPA buffer (ThermoFisher Scientific) per T75 flask by pipetting. Homogenates were transferred to 1.5-mL Eppendorf tubes and incubated for 20 min on ice and then centrifuged at 13,000 × *g* for 10 min at 4 °C to precipitate nuclei. The supernatants were collected in new prechilled 1.5-mL Eppendorf tubes. The protein concentration of homogenates was determined using the BCA protein assay kit (PIERCE) following the manufacturer's instructions.

To immunoprecipitate ALCAM, 50 μL Dynabeads protein G (ThermoFisher Scientific) were coupled to 10 μg of polyclonal goat anti-mouse ALCAM (R&D Systems, AF1172) or to 10 μg of irrelevant goat IgG (R&D Systems) following the manufacturer's instructions. To avoid postcoupling elution of the Ig, they were covalently attached to the beads by BS3 [bis(sulfosuccinimidyl)suberate] cross-linking agent (ThermoFisher Scientific) following the manufacturer's instructions. A total of 50 μL of the resulting anti-ALCAM Dynabeads or the irrelevant IgG control were incubated overnight with 200 μg of MBEC homogenates at 4 °C with gentle rotation. The beads were then washed four times with PBSTween 20 (0.05%). The supernatant was completely removed, and 40 μL of 1× SDS loading buffer with 2.5% β-mercaptoethanol were added to the beads and incubated 15 min at room temperature following resuspension. The beads were boiled at 95 °C for 5 min and then centrifuged at 13,000 rpm for 2 min. The supernatant was collected and migrated in SDS/PAGE, transferred to PVDF membranes, and immunostained with the corresponding antibodies.

Immunoblotting. Immunoblotting was performed as previously described (11, 63). Briefly, MBEC lysates or BBB blood vessel lysates were separated by standard SDS/PAGE, and immunoblots were analyzed with the following antibodies: goat anti-ALCAM (0.25 μg/mL, AF1172, R&D Systems); rabbit anti–ZO-1 (1:125, Invitrogen); rabbit anti–ZO-2 (1:125, Invitrogen); rabbit anti-cingulin (1:500, Thermos); rabbit anti-TARA (1:500, Thermos); mouse anti-coronin 1C (1:500, Abnova); mouse anti–β-actin (1:20,000, Sigma-Aldrich); mouse anti-TPM (1:500, Sigma-Aldrich); rabbit anti-occludin (1:250, Invitrogen); rabbit anti-ezrin (1 μg/mL, Abcam); and rabbit anti–syntenin-1 (1:500, Bioss). Horseradish peroxidase-conjugated secondary antibodies (Dako) and the ECL system (Amersham Biosciences) were used to detect specific binding, and anti–β-actin (Sigma-Aldrich) served as a loading control. Digital images obtained with the Bio-Rad Gel Doc system were used for band intensity analysis.

TEER Measurement. Barrier properties of confluent monolayers formed by pMBMECs (59) from ALCAM KO or WT mice grown on filter inserts (0.4-μm pore size, 8.36-mm diameter; ThinCertTM, Greiner Bio-One, Vitaris AG) were assessed by impedance TEER measurements (CellZscope R, Nanoanalytics) according to the manufacturer's instructions.

In Vitro Permeability of MBECs to Tracer Molecules. MBECs were isolated and cultured to 90% confluence in six-well plates. Then, using 0.25% trypsin diluted in PBS–EDTA (2 mM), the cells were quickly detached and plated on gelatin/collagen IV-coated, 3-μm pore size Boyden chambers at a density of 4×10^4 cells per well. Cells reached confluence after 3–4 d, at which point the culture media were changed for DMEM media supplemented with 20% FBS. After 2 h, fluorescein–isothiocyanate-labeled BSA (FITC-BSA, 66.5 kDa, Invitrogen) and Alexa 647-labeled dextran (10 kDa, Invitrogen) were added at 50 μg/mL to the upper chambers. Aliquots of 50 μL were separately harvested from each upper and lower chamber at 0 and 1 h. Experimental conditions were prepared in triplicates. The permeability of the tracers was quantified with a fluorescence multimode plate reader (Biotek, Synergy 4), which allows for the calculation of the permeability coefficient of each fluorescent marker.

In Vivo BBB Permeability. In vivo BBB permeability was assessed by measuring Cascade Blue-labeled dextran (3 kDa, Invitrogen) and dextran-TRITC (20 kDa, Sigma-Aldrich) in the CNS of mice at different time points. Mice were injected i.v. with saline, 0.9% NaCl containing 1 mg of dextran–Cascade Blue and 1 mg of dextran-TRITC. Then, 15 min later, 200 μL of blood was obtained by intracardiac puncture and placed in an EDTA-coated blood tube (Sarstedt). Immediately afterward, the mice were perfused with ice-cold saline. The brains and spinal cords were then removed and placed in 1 mL of cold PBS protected from light. The CNS samples were weighed and then homogenized using syringes and decreasing size needles. The CNS and blood proteins were precipitated with 1 mL of 60% trichloroacetic acid. The precipitates were removed by centrifugation. Fluorescence was measured using a fluorescence multimode plate reader (Biotek, Synergy 4). dextran-Cascade Blue (excitation at 557 nm, emission at 575 nm) and dextran-TRITC (excitation at 390 nm, emission at 420 nm) were measured in supernatant samples using a dark-wall, clear-bottom Cornstar 96-well plate. The quantity of dyes contained in the CNS tissue was expressed as a percentage of the fluorescence intensity found in the blood originating from the same animal, normalized based on CNS weight.

Statistical Analysis. Statistical analysis was performed using Prism software (GraphPad Software), and results are presented as the mean ± SEM. Paired or unpaired Student's *t* tests were performed when appropriate. Two-way ANOVA and Student's *t* tests were performed on the calculated AUC using individual EAE scores. Only P values < 0.05 were considered statistically significant ($*P \leq 0.05$, $**P \leq 0.01$, $***P \leq 0.001$).

ACKNOWLEDGMENTS. We thank Dr. Joshua A. Weiner and Prof. Cornelia Halin (Institute of Pharmaceutical Sciences, ETH Zurich, Zurich) for the generous gift of the activated leukocyte cell adhesion molecule (ALCAM) KO

mice; Dr. Urban Deutsch for the management of the transgenic mouse colony; and Claudia Blatti for her technical assistance with experimental autoimmune encephalomyelitis experiments (EAE). This study was supported by operating grants from the Multiple Sclerosis Society of Canada (MSSOC) (to A.P.) and the Swiss National Science Foundation Grant 133092 and ProDoc Cell Migration and the Swiss MS Society (to B.E. and R.L.). M-.A.L. holds a scholarship from Fonds de Recherche du Québec-Santé. C.L., M.C., E.G., and O.S.-L. hold scholarships and fellowships from the MSSOC. A.P. holds a Senior Scholar Award of the Fonds de Recherche du Québec-Santé and holds a senior Canada Research Chair (tier 1) in Multiple Sclerosis.

1. Cayrol R, Haqqani AS, Ifergan I, Dodelet-Devillers A, Prat A (2011) Isolation of human brain endothelial cells and characterization of lipid raft-associated proteins by mass spectroscopy. *Methods Mol Biol* 686:275–295.
2. Dodelet-Devillers A, et al. (2009) Functions of lipid raft membrane microdomains at the blood-brain barrier. *J Mol Med (Berl)* 87(8):765–774.
3. Larochelle C, Alvarez JI, Prat A (2011) How do immune cells overcome the blood-brain barrier in multiple sclerosis? *FEBS Lett* 585(23):3770–3780.
4. Tietz S, Engelhardt B (2015) Brain barriers: Crosstalk between complex tight junctions and adherens junctions. *J Cell Biol* 209(4):493–506.
5. Alvarez JI, Cayrol R, Prat A (2011) Disruption of central nervous system barriers in multiple sclerosis. *Biochim Biophys Acta* 1812(2):252–264.
6. Lécuyer MA, Kebir H, Prat A (2016) Glial influences on BBB functions and molecular players in immune cell trafficking. *Biochim Biophys Acta* 1862(3):472–482.
7. Larochelle C, et al. (2016) Immunological and pathological characterization of fatal rebound MS activity following natalizumab withdrawal. *Mult Scler* pii:1352458516641775.
8. Abadier M, et al. (2015) Cell surface levels of endothelial ICAM-1 influence the transcellular or paracellular T-cell diapedesis across the blood-brain barrier. *Eur J Immunol* 45(4):1043–1058.
9. Steiner O, et al. (2010) Differential roles for endothelial ICAM-1, ICAM-2, and VCAM-1 in shear-resistant T cell arrest, polarization, and directed crawling on blood-brain barrier endothelium. *J Immunol* 185(8):4846–4855.
10. Steffen BJ, Butcher EC, Engelhardt B (1994) Evidence for involvement of ICAM-1 and VCAM-1 in lymphocyte interaction with endothelium in experimental autoimmune encephalomyelitis in the central nervous system in the SJL/J mouse. *Am J Pathol* 145(1):189–201.
11. Cayrol R, et al. (2008) Activated leukocyte cell adhesion molecule promotes leukocyte trafficking into the central nervous system. *Nat Immunol* 9(2):137–145.
12. Lyck R, et al. (2016) ALCAM (CD166) is involved in extravasation of monocytes rather than T cells across the blood–brain barrier. *J Cereb Blood Flow Metab*, doi: 10.1177/0271678X16678639.
13. Flanagan K, et al. (2012) Laminin-411 is a vascular ligand for MCAM and facilitates TH17 cell entry into the CNS. *PLoS One* 7(7):e40443.
14. Larochelle C, et al. (2012) Melanoma cell adhesion molecule identifies encephalitogenic T lymphocytes and promotes their recruitment to the central nervous system. *Brain* 135(Pt 10):2906–2924.
15. Larochelle C, et al. (2015) Melanoma cell adhesion molecule-positive CD8 T lymphocytes mediate central nervous system inflammation. *Ann Neurol* 78(1):39–53.
16. Berg EL, McEvoy LM, Berlin C, Bargatze RF, Butcher EC (1993) L-selectin-mediated lymphocyte rolling on MAdCAM-1. *Nature* 366(6456):695–698.
17. Berlin C, et al. (1993) Alpha 4 beta 7 integrin mediates lymphocyte binding to the mucosal vascular addressin MAdCAM-1. *Cell* 74(1):185–195.
18. Lalor PF, et al. (2002) Vascular adhesion protein-1 mediates adhesion and transmigration of lymphocytes on human hepatic endothelial cells. *J Immunol* 169(2):983–992.
19. Pannecoeck R, et al. (2015) Vascular adhesion protein-1: Role in human pathology and application as a biomarker. *Crit Rev Clin Lab Sci* 52(6):284–300.
20. Ifergan I, et al. (2011) Role of Ninjurin-1 in the migration of myeloid cells to central nervous system inflammatory lesions. *Ann Neurol* 70(5):751–763.
21. Alvarez JI, et al. (2015) JAML mediates monocyte and CD8 T cell migration across the brain endothelium. *Ann Clin Transl Neurol* 2(11):1032–1037.
22. Bowen MA, et al. (1995) Cloning, mapping, and characterization of activated leukocyte-cell adhesion molecule (ALCAM), a CD6 ligand. *J Exp Med* 181(6):2213–2220.
23. Patel DD, et al. (1995) Identification and characterization of a 100-kD ligand for CD6 on human thymic epithelial cells. *J Exp Med* 181(4):1563–1568.
24. Zimmerman AW, et al. (2006) Long-term engagement of CD6 and ALCAM is essential for T-cell proliferation induced by dendritic cells. *Blood* 107(8):3212–3220.
25. Whitney GS, et al. (1995) The membrane-proximal scavenger receptor cysteine-rich domain of CD6 contains the activated leukocyte cell adhesion molecule binding site. *J Biol Chem* 270(31):18187–18190.
26. van Kempen LC, et al. (2001) Molecular basis for the homophilic activated leukocyte cell adhesion molecule (ALCAM)-ALCAM interaction. *J Biol Chem* 276(28):25783–25790.
27. Te Riet J, et al. (2007) Distinct kinetic and mechanical properties govern ALCAM-mediated interactions as shown by single-molecule force spectroscopy. *J Cell Sci* 120(Pt 22):3965–3976.
28. Wagner M, et al. (2013) ALCAM–Novel multiple sclerosis locus interfering with HLA-DRB1*1501. *J Neuroimmunol* 258(1-2):71–76.
29. Kofler DM, Severson CA, Mousissian N, De Jager PL, Hafler DA (2011) The CD6 multiple sclerosis susceptibility allele is associated with alterations in CD4+ T cell proliferation. *J Immunol* 187(6):3286–3291.
30. De Jager PL, et al.; International MS Genetics Consortium (2009) Meta-analysis of genome scans and replication identify CD6, IRF8 and TNFRSF1A as new multiple sclerosis susceptibility loci. *Nat Genet* 41(7):776–782.
31. Wagner M, et al. (2014) ALCAM and CD6–Multiple sclerosis risk factors. *J Neuroimmunol* 276(1-2):98–103.
32. Crockett ET, Remelius C, Hess K, Al-Ghawi H (2004) Gene deletion of P-Selectin and ICAM-1 does not inhibit neutrophil infiltration into peritoneal cavity following cecal ligation-puncture. *BMC Clin Pathol* 4(1):2.
33. Hobden JA, Masinick-McClellan S, Barrett RP, Bark KS, Hazlett LD (1999) Pseudomonas aeruginosa keratitis in knockout mice deficient in intercellular adhesion molecule 1. *Infect Immun* 67(2):972–975.
34. Schenkel AR, Chew TW, Muller WA (2004) Platelet endothelial cell adhesion molecule deficiency or blockade significantly reduces leukocyte emigration in a majority of mouse strains. *J Immunol* 173(10):6403–6408.
35. Mondal N, et al. (2016) Glycosphingolipids on human myeloid cells stabilize E-selectin-dependent rolling in the multistep leukocyte adhesion cascade. *Arterioscler Thromb Vasc Biol* 36(4):718–727.
36. Zou X, et al. (2005) PSGL-1 derived from human neutrophils is a high-efficiency ligand for endothelium-expressed E-selectin under flow. *Am J Physiol Cell Physiol* 289(2):C415–C424.
37. Tudor C, et al. (2014) Syntenin-1 and ezrin proteins link activated leukocyte cell adhesion molecule to the actin cytoskeleton. *J Biol Chem* 289(19):13445–13460.
38. Yao H, et al. (2011) Cocaine hijacks σ1 receptor to initiate induction of activated leukocyte cell adhesion molecule: Implication for increased monocyte adhesion and migration in the CNS. *J Neurosci* 31(16):5942–5955.
39. Williams DW, et al. (2013) Mechanisms of HIV entry into the CNS: Increased sensitivity of HIV infected CD14+CD16+ monocytes to CCL2 and key roles of CCR2, JAM-A, and ALCAM in diapedesis. *PLoS One* 8(7):e69270.
40. Masedunskas A, et al. (2006) Activated leukocyte cell adhesion molecule is a component of the endothelial junction involved in transendothelial monocyte migration. *FEBS Lett* 580(11):2637–2645.
41. Curis C, et al. (2016) Human T-lymphotropic virus type 1-induced overexpression of activated leukocyte cell adhesion molecule (ALCAM) facilitates trafficking of infected lymphocytes through the blood-brain barrier. *J Virol* 90(16):7303–7312.
42. Nummer D, et al. (2007) Role of tumor endothelium in CD4+ CD25+ regulatory T cell infiltration of human pancreatic carcinoma. *J Natl Cancer Inst* 99(15):1188–1199.
43. Muller WA, Weigl SA, Deng X, Phillips DM (1993) PECAM-1 is required for transendothelial migration of leukocytes. *J Exp Med* 178(2):449–460.
44. Schenkel AR, Mamdouh Z, Chen X, Liebman RM, Muller WA (2002) CD99 plays a major role in the migration of monocytes through endothelial junctions. *Nat Immunol* 3(2):143–150.
45. Johnson-Léger CA, Aurrand-Lions M, Beltraminelli N, Fasel N, Imhof BA (2002) Junctional adhesion molecule-2 (JAM-2) promotes lymphocyte transendothelial migration. *Blood* 100(7):2479–2486.
46. Bardin N, et al. (2001) Identification of CD146 as a component of the endothelial junction involved in the control of cell-cell cohesion. *Blood* 98(13):3677–3684.
47. Nelissen JM, Peters IM, de Grooth BG, van Kooyk Y, Figdor CG (2000) Dynamic regulation of activated leukocyte cell adhesion molecule-mediated homotypic cell adhesion through the actin cytoskeleton. *Mol Biol Cell* 11(6):2057–2068.
48. Te Riet J, et al. (2014) Dynamic coupling of ALCAM to the actin cortex strengthens cell adhesion to CD6. *J Cell Sci* 127(Pt 7):1595–1606.
49. Zimmerman AW, et al. (2004) Cytoskeletal restraints regulate homotypic ALCAM-mediated adhesion through PKCalpha independently of Rho-like GTPases. *J Cell Sci* 117(Pt 13):2841–2852.
50. Dykstra M, Cherukuri A, Sohn HW, Tzeng SJ, Pierce SK (2003) Location is everything: Lipid rafts and immune cell signaling. *Annu Rev Immunol* 21:457–481.
51. Tilghman RW, Hoover RL (2002) E-selectin and ICAM-1 are incorporated into detergent-insoluble membrane domains following clustering in endothelial cells. *FEBS Lett* 525(1-3):83–87.
52. Head BP, Patel HH, Insel PA (2014) Interaction of membrane/lipid rafts with the cytoskeleton: Impact on signaling and function: Membrane/lipid rafts, mediators of cytoskeletal arrangement and cell signaling. *Biochim Biophys Acta* 1838(2):532–545.
53. Ofori-Acquah SF, King J, Voelkel N, Schaphorst KL, Stevens T (2008) Heterogeneity of barrier function in the lung reflects diversity in endothelial cell junctions. *Microvasc Res* 75(3):391–402.
54. Gilsanz A, et al. (2013) ALCAM/CD166 adhesive function is regulated by the tetraspanin CD9. *Cell Mol Life Sci* 70(3):475–493.
55. Gutiérrez-López MD, et al. (2011) The sheddase activity of ADAM17/TACE is regulated by the tetraspanin CD9. *Cell Mol Life Sci* 68(19):3275–3292.
56. Klein-Soyer C, Azorsa DO, Cazenave JP, Lanza F (2000) CD9 participates in endothelial cell migration during in vitro wound repair. *Arterioscler Thromb Vasc Biol* 20(2):360–369.
57. Weiner JA, et al. (2004) Axon fasciculation defects and retinal dysplasias in mice lacking the immunoglobulin superfamily adhesion molecule BEN/ALCAM/SC1. *Mol Cell Neurosci* 27(1):59–69.
58. Ifergan I, et al. (2011) Central nervous system recruitment of effector memory CD8+ T lymphocytes during neuroinflammation is dependent on α4 integrin. *Brain* 134(Pt 12):3560–3577.
59. Lyck R, et al. (2009) Culture-induced changes in blood-brain barrier transcriptome: Implications for amino-acid transporters in vivo. *J Cereb Blood Flow Metab* 29(9):1491–1502.
60. Ifergan I, et al. (2006) Statins reduce human blood-brain barrier permeability and restrict leukocyte migration: Relevance to multiple sclerosis. *Ann Neurol* 60(1):45–55.
61. Kebir H, et al. (2009) Preferential recruitment of interferon-gamma-expressing TH17 cells in multiple sclerosis. *Ann Neurol* 66(3):390–402.
62. Alvarez JI, et al. (2011) The Hedgehog pathway promotes blood-brain barrier integrity and CNS immune quiescence. *Science* 334(6063):1727–1731.
63. Podjaski C, et al. (2015) Netrin 1 regulates blood-brain barrier function and neuroinflammation. *Brain* 138(Pt 6):1598–1612.